Renal Ca^{2+} wasting, hyperabsorption, and reduced bone thickness in mice lacking TRPV5

Joost G.J. Hoenderop,[1] Johannes P.T.M. van Leeuwen,[2] Bram C.J. van der Eerden,[2] Ferry F.J. Kersten,[1] Annemiete W.C.M. van der Kemp,[1] Anne-Marie Mérillat,[4] Jan H. Waarsing,[3] Bernard C. Rossier,[4] Volker Vallon,[5] Edith Hummler,[4] and René J.M. Bindels[1]

[1]Department of Physiology, Nijmegen Center for Molecular Life Sciences, University Medical Center Nijmegen, Nijmegen, The Netherlands
[2]Department of Internal Medicine and
[3]Department of Orthopaedics, Erasmus MC, Rotterdam, The Netherlands
[4]Institut de Pharmacologie et de Toxicologie, Université de Lausanne, Lausanne, Switzerland
[5]Department of Pharmacology and Toxicology, University of Tübingen, Tübingen, Germany

Ca^{2+} ions play a fundamental role in many cellular processes, and the extracellular concentration of Ca^{2+} is kept under strict control to allow the proper physiological functions to take place. The kidney, small intestine, and bone determine the Ca^{2+} flux to the extracellular Ca^{2+} pool in a concerted fashion. Transient receptor potential (TRP) cation channel subfamily V, members 5 and 6 (TRPV5 and TRPV6) have recently been postulated to be the molecular gatekeepers facilitating Ca^{2+} influx in these tissues and are members of the TRP family, which mediates diverse biological effects ranging from pain perception to male aggression. Genetic ablation of TRPV5 in the mouse allowed us to investigate the function of this novel Ca^{2+} channel in maintaining the Ca^{2+} balance. Here, we demonstrate that mice lacking TRPV5 display diminished active Ca^{2+} reabsorption despite enhanced vitamin D levels, causing severe hypercalciuria. In vivo micropuncture experiments demonstrated that Ca^{2+} reabsorption was malfunctioning within the early part of the distal convolution, exactly where TRPV5 is localized. In addition, compensatory hyperabsorption of dietary Ca^{2+} was measured in TRPV5 knockout mice. Furthermore, the knockout mice exhibited significant disturbances in bone structure, including reduced trabecular and cortical bone thickness. These data demonstrate the key function of TRPV5 in active Ca^{2+} reabsorption and its essential role in the Ca^{2+} homeostasis.

J. Clin. Invest. **112**:1906–1914 (2003). doi:10.1172/JCI200319826.

Received for publication August 18, 2003, and accepted in revised form October 21, 2003.

Address correspondence to: René J.M. Bindels, 160 Cell Physiology, University Medical Center Nijmegen, P.O. Box 9101, NL-6500 HB Nijmegen, The Netherlands. Phone: 31-24-3614211; Fax: 31-24-3616413; E-mail: r.bindels@ncmls.kun.nl.
Johannes P.T.M. van Leeuwen, Edith Hummler, and René J.M. Bindels contributed equally to this work.

Conflict of interest: The authors have declared that no conflict of interest exists.

Nonstandard abbreviations used: parathyroid hormone (PTH); 1,25-dihydroxycholecalciferol (1,25-$(OH)_2D_3$); transient receptor potential (TRP); TRP cation channel subfamily V, member 5 (TRPV5); TRP cation channel subfamily V, member 6 (TRPV6); last loop of proximal tubules (LPT); hypoxanthine-guanine phosphoribosyl transferase (HPRT); bone volume (BV); total bone marrow volume including trabeculae (TV); trabecular bone volume fraction (BV/TV); trabecular thickness (Tb.Th); trabecular number (Tb.N); connectivity density (CD); structure model index (SMI); cortical volume (Ct.V); endocortical volume (Ec.V); total diaphyseal volume (Dp.V), cortical thickness (Ct.Th); cortical bone volume fraction (Ct.V/Dp.V); moment of inertia (MOI); Tartrate-resistant acid phosphatase (TRAP); number of osteoclasts per bone surface area (N.Oc/BS); surface area of osteoclasts per bone surface area (Oc.S/BS); arginine vasopressin (AVP); Na^+-Ca^{2+} exchanger (NCX1); vitamin D receptor (VDR).

Introduction

Ca^{2+} is the most abundant cation in the human body and serves a number of important physiological functions, including fertilization, synaptic transmission, muscle contraction, blood clotting, and bone mineralization. The extracellular Ca^{2+} concentration is controlled by the kidney, intestine, and bone through the action of the calciotropic hormones, including parathyroid hormone (PTH) and 1,25-dihydroxycholecalciferol (1,25-$(OH)_2D_3$). In humans, the daily dietary Ca^{2+} intake is less than 1,000 mg, of which only 30% is absorbed in the intestinal tract. This percentage is significantly enhanced during growth, pregnancy, and lactation by increased levels of circulating 1,25-$(OH)_2D_3$. Although there is continuous turnover of bone mass, there is no net gain or loss of Ca^{2+} from bone in a young and healthy individual. This indicates that healthy adults excrete a maximum of 300 mg Ca^{2+} in the urine to balance the intestinal Ca^{2+} uptake and that the remaining 98% of the Ca^{2+} filtered in the glomeruli is reabsorbed along the nephron. The molecular mechanism responsible for Ca^{2+} absorption in the small intestine and the kidney was elusive for a long time.

The cloning of transient receptor potential (TRP) cation channel subfamily V, member 5 (TRPV5; originally called ECaC1) from vitamin D–responsive rabbit renal epithelial cells (1) and TRP cation channel subfamily V, member 6 (TRPV6; originally called CaT1) from rat duodenum (2) has ignited research into transcellular Ca^{2+} (re)absorption at the molecular level (1). Mammals harbor at least 21 genes of the so-called TRP channels, whose functions remain mostly unknown (3). TRPV5 has been implicated as the Ca^{2+} influx channel in the process of vitamin D–responsive active Ca^{2+} reabsorption in the kidney (1, 4). In comparison, the TRPV5 homolog TRPV6, which displays an amino acid sequence identity of about 75% to TRPV5, has been postulated to be the Ca^{2+} influx channel facilitating Ca^{2+} absorption in enterocytes (2). TRPV6 is ubiquitously expressed and has been implicated as part of the capacitative Ca^{2+} entry mechanism and, therefore, intracellular Ca^{2+} signaling (5). TRPV5 and TRPV6 are Ca^{2+}-selective channels that belong, together with the temperature-activated vanilloid receptors, to the TRPV subfamily (3, 4). Genomic cloning has demonstrated that TRPV5 and TRPV6 form a unique pair of novel Ca^{2+} channels that are transcribed from distinct genes juxtaposed on human chromosome 7q35 (4).

The present study investigated the physiological function of TRPV5 by the generation and characterization of TRPV5 knockout mice. Here, we demonstrate that the new TRP member TRPV5 is the gatekeeper in active Ca^{2+} reabsorption in the kidney. Ablation of the *TRPV5* gene seriously disturbs renal Ca^{2+} handling, resulting in compensatory intestinal hyperabsorption and bone abnormalities.

Methods

Generation of TRPV5-null mice. The *TRPV5* gene was cloned from a 129/Sv mouse genomic library. For TRPV5 gene information, see GenBank accession number *AF336378*. The following fragments were then subcloned into a modified lox-targeting vector containing three *loxP* sites (6). First, a 1.2-kb 5′ homology fragment was inserted upstream of the 5′ *loxP* site in the pAT-FRT- K13 plasmid (kindly provided by A. Trumpp, University of California at San Francisco, San Francisco, California, USA) using long-range PCR with Takara polymerase (Takara Biomedical, Tokyo, Japan). For 3′ homology, a PCR-amplified 4-kb fragment was subcloned in the *Pme*I site of the pBS KS(+) targeting vector adjacent to the negative selection gene *HSV-Tk* (kindly provided by F. Radtke, University of Lausanne). Subsequently, for the functional channel region, a 600-bp PCR fragment containing exon 13 encoding the entire pore-forming region of the TRPV5 protein was cloned into the *Not*I and *Asc*I sites by exchange of the neomycin-flanked *loxP* cassette. Finally, these two vectors were combined to construct the neomycin-*loxP*–targeting vector. To this end, the *Xho*I–*Not*I fragment from the pAT-FRT-K13 plasmid, containing the 5′ homology, the frt-flanked neomycin cassette, and the 5′ *loxP* site, was cloned into the *Sal*I and *Not*I site of the pBS KS(+) vector upstream of the vital region. Electroporation and selection of targeted clones has been described (7). A recombinant ES cell was used to generate chimeras, allowing germline transmission of the mutant allele ($TRPV5^{loxneo}$). Heterozygous mice ($TRPV5^{+/-}$) harboring a null allele were obtained by breeding $TRPV5^{loxneo}$ mice with a germline EIIa-cre-deletor strain (8). Offspring of heterozygous null mutants were subsequently intercrossed to obtain the $TRPV5^{+/+}$, $TRPV5^{+/-}$, and $TRPV5^{-/-}$ mice used in this study. The frt-flanked neomycin cassette was not deleted in these mice. In all experiments, B6.129$TRPV5^{-/-}$,N_2 mice were compared with their $TRPV5^{+/+}$ and $TRPV5^{+/-}$ littermates. Adult mice 8–9 weeks old, fed ad libitum, were placed in metabolic cages for 48 hours (Techniplast, Buguggiate, Italy). Food and fluid intake was monitored by weighing "sipper" bottles before and after the test period. Mice were allowed to adapt to these cages for 1 day, and then 24-hour urine samples were collected. The animal ethics board of the University Medical Center Nijmegen approved all experimental procedures.

Genotyping. Genotyping was confirmed by Southern blot analysis of tail-derived DNA digested with *Bam*HI and hybridized to a 5′ probe that demonstrated successful generation of the $TRPV5^{loxneo}$ and $TRPV5^{null}$ alleles (Figure 1, a and b). Heterozygous mice harbor a band of 5.8 kb plus a 4.6-kb endogenous wild-type band. Subsequently, genotypes were determined by PCR with primers A (5′-GCCAAGTTCTAATTCCATCAGAAG-3′) and B (5′-CTCCTATTCCCTGAAACCGCA-3′) to detect the null allele; and C (5′-TTCCCCAACTGTTCTTCCTGG-3′) and D (5′-AGATCCTCCAGTGTCTCATGCT-3′) to detect the wild-type allele (Figure 1a). The presence or absence of a 500-bp fragment (null allele) or 483-bp fragment (wild-type allele) identifies animals with –/–, +/+, and +/– genotypes (Figure 1c).

Serum and urine analysis. Serum 1,25-$(OH)_2D_3$, PTH, osteocalcin concentrations, and alkaline phosphatase were assayed according standard procedures. Mouse serum PTH levels were measured using a kit from Immunotopics Inc. (San Clemente, California, USA). Deoxypyrillinodine was analyzed in urine (Biometra, San Francisco, USA). Electrolytes in urine were measured using an Autoanalyzer (Hitachi, Laval, Quebec, Canada).

Micropuncture. Mice anesthetized by inactin/ketamine were prepared for micropuncture as described (9). For assessment of GFR of both kidneys and of single nephrons, [^{3}H]inulin was infused intravenously. Urine was collected using a bladder catheter. The left kidney was prepared for micropuncture. On the kidney surface, the last loop of proximal tubules (LPTs) or the distal convolutions were identified and punctured for quantitative collection of tubular fluid. Tubular fluid volume was determined from column length in a constant bore capillary. The tubular fluid concentration of K^+ was determined by a micro-flame photometer (Department of Pharmacology, University of Tübingen) (9) and

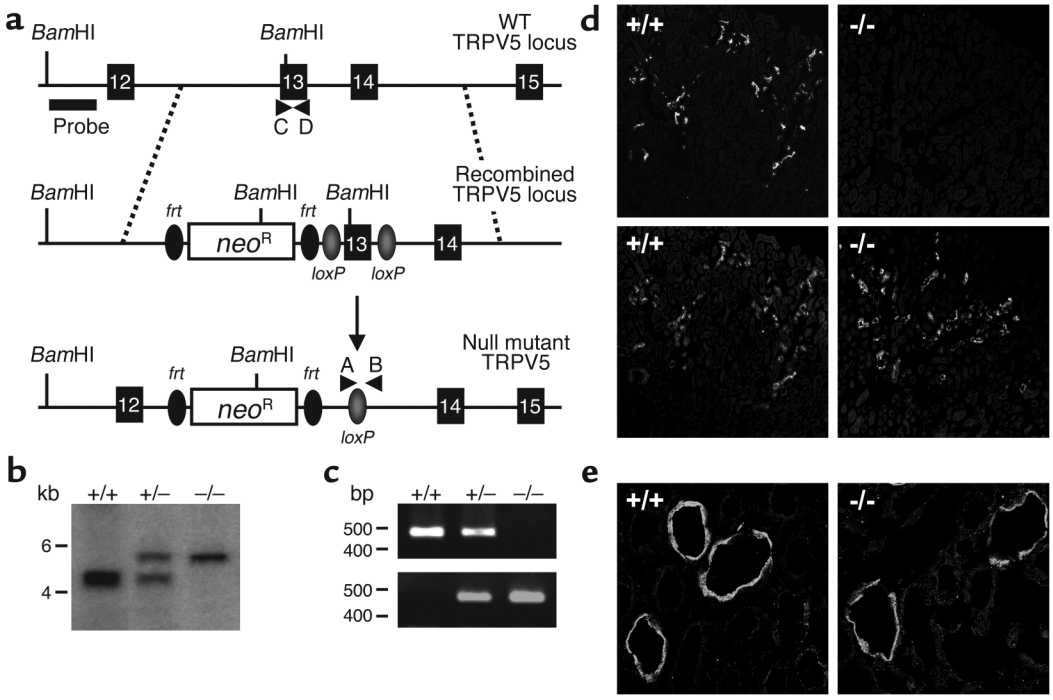

Figure 1
Creation of null mutant mice for the *TRPV5* gene locus. (**a**) Targeted inactivation of the *TRPV5* gene. Top, exon 13, encoding the pore-forming unit of TRPV5, is flanked by *loxP* sites. Middle, recombined TRPV5^{loxneo} locus. Bottom, targeted allele in which exon 13 is deleted by Cre recombinase. Black boxes indicate exons; probe and genotype primers (A–D) are depicted. neo^R, neomycin resistance cassette. (**b**) Representative Southern blot analysis of *Bam*HI-digested tail-derived DNA isolated from *TRPV5*$^{+/+}$, *TRPV5*$^{+/-}$, and *TRPV5*$^{-/-}$ mice. (**c**) Identification of mouse genotype by PCR analysis of tail-derived DNA. The PCR product in the upper gel shows the presence of the wild-type allele (+/+) using primers C and D; the lower gel shows the knockout allele (–/–) using primers A and B. Both alleles are detected in heterozygous animals (+/–). (**d**) TRPV5 (top images) and kallikrein (lower images) immunohistochemical costaining of kidney cortex from *TRPV5*$^{+/+}$ and *TRPV5*$^{-/-}$ mice. (**e**) Immunopositive TRPV6 staining of renal distal tubules from *TRPV5*$^{+/+}$ and *TRPV5*$^{-/-}$ mice. A color version of this figure is available online as Supplementary Figure 1 (http://www.jci.org/cgi/content/full/112/12/1906/DC1).

of Ca^{2+}, by a flow-through microfluorometer (NanoFlo; WPI, Sarasota, Florida, USA) using Fluo-3 (MoBiTec, Göttingen, Germany) for detection (10, 11).

Immunohistochemistry. Antibodies against TRPV5 and TRPV6 were obtained by immunization of guinea pigs and rabbits, respectively, with channel-specific peptides as described previously (12). Kidneys from *TRPV5*$^{+/+}$ and *TRPV5*$^{-/-}$ mice were cut into pieces, placed in 1% (weight/volume) periodate-lysine-paraformaldehyde fixative for 2 hours, and incubated overnight in phosphate-buffered saline containing 15% (weight/volume) sucrose. Subsequently, samples were frozen in liquid nitrogen and sections 5–7 μm in thickness were used for different staining procedures as described previously (12). Rabbit anti-kallikrein was purchased from Calbiochem (San Diego, California, USA). All negative controls, including sections incubated with preimmune serum, subjected to preabsorption for 1 hour with 10 μg/ml TRPV5 or TRPV6 peptide, or incubated solely with conjugated secondary antibodies, were devoid of any staining. Photographs were taken with a Bio-Rad MRC 1000 confocal laser-scanning microscope.

Quantitative real-time PCR analysis. Total RNA was extracted from kidney and duodenal tissues using the TriZol Total RNA Isolation Reagent (Gibco BRL, Breda, The Netherlands). The RNA was subjected to DNAse treatment to prevent genomic DNA contamination. Thereafter, 2 μg RNA was reverse-transcribed by Moloney murine leukemia virus reverse transcriptase (Gibco BRL) as described previously (13). The cDNA obtained was used to determine TRPV6, calbindin-D_{28K}, calbindin-D_{9K}, and NCX1 mRNA expression levels, as well as mRNA levels of the housekeeping gene hypoxanthine-guanine phosphoribosyl transferase (HPRT) as an endogenous control, as described previously (13). Expression levels were quantified by real-time quantitative PCR on an ABI Prism 7700 Sequence Detection System (PE Biosystems, Rotkreuz, Switzerland).

In vivo $^{45}Ca^{2+}$ absorption assay. Ca^{2+} absorption was assessed by measuring serum $^{45}Ca^{2+}$ at early time points after oral gavage. Mice were fasted 12 hours before the test. Animals were hemodynamically stable under anesthesia (urethane, 1.4 mg/g body weight) during the experiment. The solution used to measure Ca^{2+} absorption contained 0.1 mM $CaCl_2$, 125 mM NaCl, 17 mM Tris, and 1.8 g/l fructose and was enriched with 20 μCi $^{45}CaCl_2$/ml (18 Ci/g; New England Nuclear, Newton, Massachusetts, USA). For the oral tests, 15 μl/g body

weight of this solution was administrated by gavage as described previously (14). Blood samples were obtained at indicated time intervals (Figure 3c). Serum (10 μl) was analyzed by liquid scintillation counting. The change in the plasma Ca^{2+} concentration was calculated from the $^{45}Ca^{2+}$ content of the plasma samples and the specific activity of the administrated Ca^{2+}.

Bone analysis. Femurs from 8- to 9-week-old *TRPV5*$^{+/+}$ mice (females, n = 9; males, n = 5) and *TRPV5*$^{-/-}$ mice (females, n = 8; males, n = 5) were scanned using the SkyScan 1072 microtomograph (SkyScan, Antwerp, Belgium). Scans were processed and a three-dimensional morphometric analysis of the bone was performed, using free software of the 3D-Calculator project (http://www.eur.nl/fgg/orthopaedics/Downloads.html). Measured parameters were expressed according to bone histomorphometry nomenclature (15). In the femoral head, bone volume (BV), total bone marrow volume including trabeculae (TV), trabecular bone volume fraction (BV/TV), trabecular thickness (Tb.Th) (16), trabecular number (Tb.N) (16), connectivity density (CD) (measure of the interconnectivity of the trabecular network; ref 17), and structure model index (SMI) (predominance of the shape of the trabeculae; 0 = plate-like; 3 = rod-like; ref. 18) were determined. In the diaphysis, calculations were performed with regard to cortical volume (Ct.V), endocortical volume (Ec.V), total diaphyseal volume (Dp.V) (sum of Ct.V and Ec.V), cortical thickness (Ct.Th) and cortical bone volume fraction (Ct.V/Dp.V) (16), and moment of inertia (MOI) (measure of the geometrical distribution indicative of the mechanical strength per transversal cross-section). Dissected femurs were routinely processed for plastic embedding. "Plastified" bone sections were deacrylated and rehydrated. Tartrate-resistant acid phosphatase (TRAP) staining was used to specifically stain osteoclasts red, as described (19). The number and surface area of osteoclasts per bone surface area (N.Oc/BS and Oc.S/BS, respectively) were determined in the femoral metaphysis using the Bioquant Novoprime digital-imaging software (Bioquant, Nashville, Tennessee, USA).

Statistics. Data are expressed as means ± SEM. Statistical comparisons were tested by one-way analysis of variance (ANOVA). P values less than 0.05 were considered statistically significant. All analyses were performed using the StatView Statistical Package software (Power PC version 4.51; Berkeley, California, USA) on a Macintosh computer.

Results and Discussion

Genetic ablation of TRPV5 in the mouse allowed us to investigate the requirement of TRPV5 functioning in maintaining the Ca^{2+} balance. The conditional targeting strategy was aimed at deleting the functionally critical region of the protein that encodes exon 13, comprising the entire pore region, using Cre-loxP–mediated recombination (Figure 1a). This procedure will allow the engineering of tissue-specific TRPV5 knockout mice strains in the near future, but in the present study TRPV5 null allele mutants were generated to address the overall function of this channel. To this end, TRPV5$^{loxneo/+}$ and EIIa-cre transgenic mice were crossed (8). The murine *TRPV5* gene is encoded by 15 exons and spans about 15 kb (GenBank accession number, AF336378). Southern blot together with PCR analysis demonstrated the deletion of pore-encoding exon 13, as shown in Figure 1, b and c. Immunohistochemical costaining of kidney cortex using antibodies against TRPV5 and kallikrein, a specific maker for distal convolution that comprises distal convoluted and connecting tubules (20), confirmed that the mutant TRPV5 allele was inactivated (Figure 1d). Importantly, ablation of the TRPV5 locus did not affect renal TRPV6 expression, confirming the gene-specific inactivation of TRPV5 (Figure 1e).

Gross observation revealed no obvious phenotype in the TRPV5-null mice. *TRPV5*$^{-/-}$ and *TRPV5*$^{+/-}$ mice were fertile and had similar average litter sizes (Figure 2a). *TRPV5*$^{-/-}$ pups nursed without aid and thrived to adulthood at a rate similar to that of wild-type mice, as assessed by size and weight at sexual maturity. *TRPV5*$^{-/-}$ females displayed normal maternal behaviors such as crouching and nursing, and

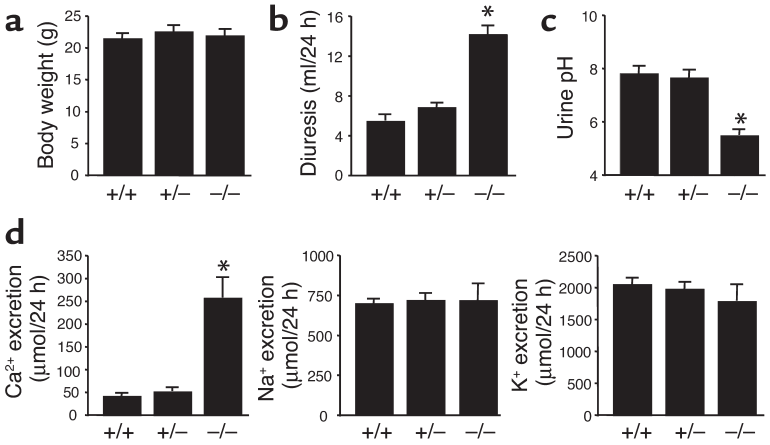

Figure 2
Phenotypic characterization of TRPV5 knockout mice. (**a**) Body weights at an age of 8 weeks of *TRPV5*$^{+/+}$, *TRPV5*$^{+/-}$, and *TRPV5*$^{-/-}$ mice (n = 29–43 mice). (**b**) The 24-hour urine volumes obtained from mice maintained in metabolic cages (n = 9 mice, three mice per cage). (**c**) Analysis of pH of urine obtained from *TRPV5*$^{+/+}$, *TRPV5*$^{+/-}$, and *TRPV5*$^{-/-}$ mice (n = 9 mice, three mice per cage). (**d**) Total excretion of Ca^{2+}, Na^+, and K^+ in *TRPV5*$^{+/+}$, *TRPV5*$^{+/-}$, and *TRPV5*$^{-/-}$ mice (n = 9 mice, three mice per cage). Of note, *TRPV5*$^{+/-}$ mice were similar to *TRPV5*$^{+/+}$ mice for the parameters measured. Data are averaged values ± SEM from mice at an age of 8 weeks. *P < 0.05, significant difference from *TRPV5*$^{+/+}$ mice.

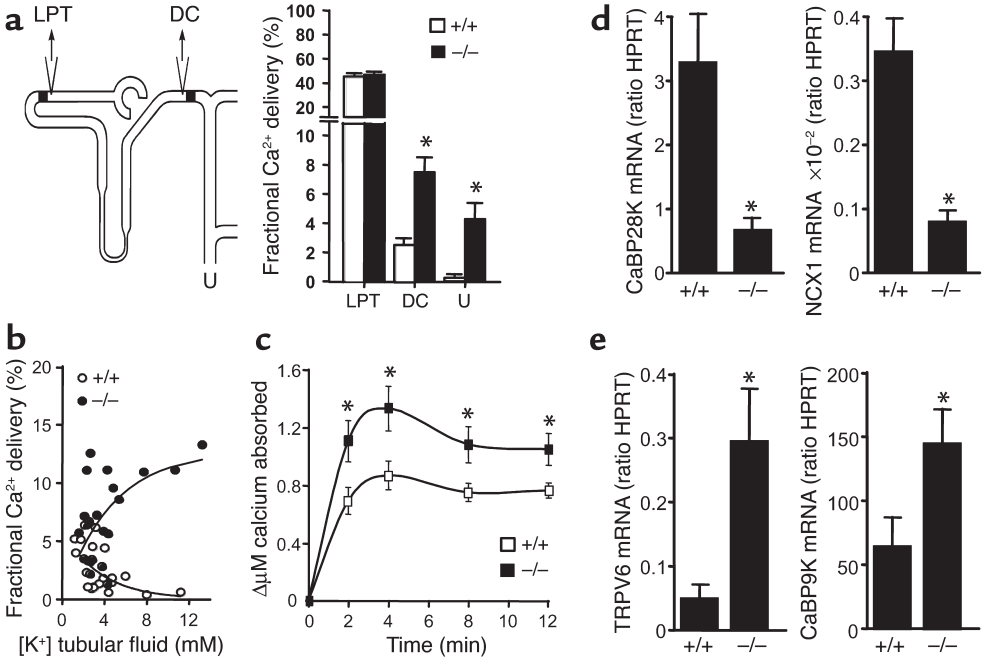

Figure 3

Renal and duodenal Ca^{2+} transport assays. (**a**) Fractional Ca^{2+} delivery to the LPT, to the distal convolution (DC), and to urine (U), measured by micropuncture experiments in *TRPV5*$^{+/+}$ and *TRPV5*$^{-/-}$ mice. (**b**) Relation between K^+ concentration in tubular fluid of the distal convolution and fractional Ca^{2+} delivery to these sites. Low K^+ concentrations indicate early puncture sites and high K^+ concentrations late aspects of distal convolution (2). Values are means ± SEM of six mice per group for urine data and of 19–24 nephrons per group for LPT and distal convolution collections. *$P < 0.05$ versus *TRPV5*$^{+/+}$. (**c**) Changes in serum Ca^{2+} (ΔμM) within 10 minutes of administration of $^{45}Ca^{2+}$ by oral gavage in *TRPV5*$^{+/+}$ and *TRPV5*$^{-/-}$ mice ($n = 12$). Data are averaged values ± SEM from mice 8 weeks old. *$P < 0.05$, significant difference from wild-type mice. (**d**) Expression of calbindin-D_{28K} and NCX1 mRNA in kidney cortexes of *TRPV5*$^{+/+}$ and *TRPV5*$^{-/-}$ mice ($n = 9$), assessed by quantitative real-time PCR analysis and calculated as a ratio to HPRT RNA. (**e**) Expression of TRPV6 and calbindin-D_{9K} mRNA in duodenums of *TRPV5*$^{+/+}$ and *TRPV5*$^{-/-}$ mice, assessed by quantitative real-time PCR analysis and calculated as a ratio to the HPRT RNA ($n = 9$).

transfer of a nursing female to a new cage initiated nest-building activity and efficient pup retrieval.

TRPV5$^{+/+}$, *TRPV5*$^{+/-}$, and *TRPV5*$^{-/-}$ mice were housed for 48 hours in metabolic cages (three mice per cage), and urine and serum samples were collected to investigate whether the electrolyte metabolism was disturbed. Polyuria was consistently observed in *TRPV5*$^{-/-}$ mice compared with heterozygous mutants and wild-type littermates (Figure 2b). Importantly, *TRPV5*$^{-/-}$ mice displayed a significant calciuresis, as they excreted about six times more Ca^{2+} in their urine than did their *TRPV5*$^{+/+}$ and *TRPV5*$^{+/-}$ littermates (Figure 2d, left panel). The urinary Ca^{2+} concentration of the knockout mice reached values as high as 20 mM, compared with 6 mM for *TRPV5*$^{+/+}$ littermates. In addition, urinary phosphate excretion was significantly increased in *TRPV5*$^{-/-}$ mice compared with that of *TRPV5*$^{+/+}$ mice (512 ± 30 μmol and 327 ± 25 μmol per 24 hours per three mice, respectively; $n = 6$, $P < 0.05$). Polyuria facilitates the excretion of large quantities of Ca^{2+} by reducing the potential risk of Ca^{2+} precipitation. It has been demonstrated that a high luminal Ca^{2+} concentration activates the calcium-sensing receptor in the apical membrane of the inner medullary collecting duct. As a consequence, the arginine vasopressin–elicited (AVP-elicited) water permeability is blunted to prevent a further rise in urinary Ca^{2+} concentration and possibly stone formation (21). Hypercalciuria-induced polyuria has been observed in humans and animal models (22–24). Notably, *TRPV5*$^{-/-}$ mice produced urine that was significantly more acidic than that of their *TRPV5*$^{+/+}$ and *TRPV5*$^{+/-}$ littermates (Figure 2c). Acidification of the urine is known to prevent renal stone formation in hypercalciuria, as Ca^{2+} oxalate stones cannot be formed at a pH of 5–6 (25). Neutralization of the acidic urine obtained from *TRPV5*$^{-/-}$ mice resulted in the development of large crystals, confirming that acidification of the urine of the knockout mice is crucial for the prevention of kidney stone formation. A better understanding of the molecular mechanism by which hypercalciuria occurs will be important for the development of clinical tools that may lead to screening of families of "stone formers" before the onset of overt disease and to early treatment.

A primary renal origin of the observed calciuresis was supported by the fact that hypercalciuria persisted when *TRPV5*$^{-/-}$ mice consumed a Ca^{2+}-deficient diet for 1 week (data not shown). Furthermore, the GFR was not different between *TRPV5*$^{-/-}$ and *TRPV5*$^{+/+}$ mice (0.31 ± 0.01 ml/min and 0.30 ± 0.07 ml/min, respectively; $n = 6$), indicating a primary defect in renal Ca^{2+} reabsorption as the cause of calciuresis in *TRPV5*$^{-/-}$ mice.

To localize the site of defective Ca^{2+} reabsorption along the nephron, we performed micropuncture studies (9–11) in anesthetized *TRPV5*$^{-/-}$ and *TRPV5*$^{+/+}$ mice (Figure 3a). Confirming the results of the experiments in the metabolic cages, *TRPV5*$^{-/-}$ mice showed calciuresis as a consequence of reduced renal Ca^{2+} reabsorption. Quantitative free-flow collection of tubular fluid revealed unaffected Ca^{2+} reabsorption in *TRPV5*$^{-/-}$ mice up to the LPT. In contrast, mean Ca^{2+} delivery to puncturing sites within the distal convolution was significantly enhanced in *TRPV5*$^{-/-}$ mice.

Because K^+ secretion occurs along the distal nephron sites accessible to micropuncture (together with water reabsorption in the connecting tubule and cortical collecting duct), the distal luminal [K^+] was used as an indicator of the distal collection site (Figure 3b). Based on the shape of the relationship between distal luminal [K^+] and fractional Ca^{2+} delivery, it is evident that, in TRPV5$^{-/-}$ mice, in contrast to *TRPV5*$^{+/+}$ mice, fractional Ca^{2+} delivery increases with higher [K^+], indicating a defect in Ca^{2+} reabsorption along the distal convolution, which is consistent with the expression site of TRPV5. Given the potential internephron variations, the observation that some nephrons of *TRPV5*$^{-/-}$ mice with low luminal [K^+] exhibit low and some high fractional Ca^{2+} delivery is consistent with a rapid increase in luminal Ca^{2+} delivery along the early distal convolutions of mice lacking TRPV5. The increase in mean fractional Ca^{2+} delivery with increasing luminal [K^+] in *TRPV5*$^{-/-}$ mice cannot be explained by a simple lack of Ca^{2+} reabsorption, but would be consistent with Ca^{2+} back-leak into the lumen in the absence of transcellular reabsorption. In comparison, if the primary Ca^{2+} reabsorption defect were upstream of the distal convolution, for example, in the thick limb of Henle's loop, then fractional Ca^{2+} delivery should be enhanced in *TRPV5*$^{-/-}$ mice distal nephrons irrespective of the luminal [K^+]. This contrasts with the observation made in the *TRPV5*$^{-/-}$ mice, indicating that the transport defect is localized primarily in the distal convolution. The fractional delivery of Na^+ to the distal convolution was not significantly different between *TRPV5*$^{-/-}$ and *TRPV5*$^{+/+}$ mice (4 ± 1% vs. 5 ± 1%, respectively; $n = 6$, $P > 0.2$), which argues against the idea that a primary decrease in Na^+ reabsorption upstream of the distal convolution indirectly influences Ca^{2+} reabsorption.

In the Ca^{2+}-reabsorbing epithelial cells of the distal convolution, the influx of Ca^{2+} is rapidly buffered by cytosolic calcium-binding proteins, that is, calbindin-D_{28K} and calbindin-D_{9K}, and the bound Ca^{2+} diffuses to the basolateral membrane where a Na^+-Ca^{2+} exchanger (NCX1) and, to a lesser extent, an ATP-dependent Ca^{2+}

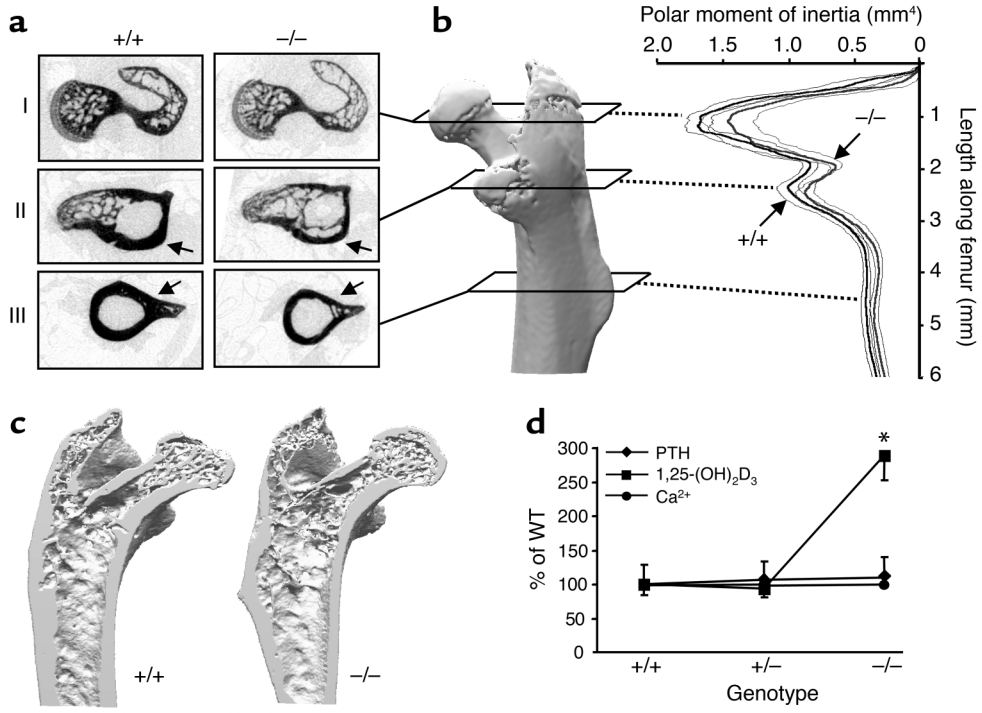

Figure 4

Bone phenotypes of female and male *TRPV5*$^{+/+}$ and *TRPV5*$^{-/-}$ mice. (**a**) Representative cross-sectional x-ray images of the femoral head (I), the lesser trochanter (II), and the diaphysis (III) in *TRPV5*$^{+/+}$ and *TRPV5*$^{-/-}$ mice. Note the decreased cortical bone width in the trochanter and diaphysis (arrows). (**b**) MOI as a parameter of bone quality. (**c**) Three-dimensional reconstruction of femurs from *TRPV5*$^{+/+}$ and *TRPV5*$^{-/-}$ mice. Note the reduced cortical and Tb.Th in *TRPV5*$^{-/-}$ mice. (**d**) Changes in serum levels of 1,25-$(OH)_2D_3$, PTH, and Ca^{2+} in *TRPV5*$^{+/+}$, *TRPV5*$^{+/-}$, and *TRPV5*$^{-/-}$ mice. Values are expressed as percentage of *TRPV5*$^{+/+}$ values ± SEM. The absolute values for PTH are *TRPV5*$^{+/+}$, 55 ± 15 pg/ml; *TRPV5*$^{+/-}$, 59 ± 14 pg/ml; and *TRPV5*$^{-/-}$, 60 ± 16 pg/ml; for 1,25-$(OH)_2D_3$, *TRPV5*$^{+/+}$, 239 ± 38 pmol/l; *TRPV5*$^{+/-}$, 225 ± 32 pmol/l; *TRPV5*$^{-/-}$, 691 ± 88 pmol/l; and for free Ca^{2+} concentration, *TRPV5*$^{+/+}$, 1.20 ± 0.02 mM; *TRPV5*$^{+/-}$, 1.25 ± 0.03 mM; and *TRPV5*$^{-/-}$, 1.20 ± 0.03 mM. *$P < 0.05$, significant difference from wild-type mice.

Table 1
Bone analysis of *TRPV5*$^{+/+}$ and *TRPV5*$^{-/-}$ mice

		Females		Males	
		+/+	−/−	+/+	−/−
Femoral head	BV/TV (%)	20.1 ± 1.96	17.7 ± 1.00	24.7 ± 1.13	24.0 ± 1.09
	Tb.Th (μm)	71.1 ± 1.2	63.8 ± 1.6^{A}	73.9 ± 1.7	66.5 ± 1.5^{A}
	Tb.N	283 ± 23.8	277 ± 13.5	362 ± 22.4	333 ± 10.4
	CD (mm^{-3})	0.16 ± 0.02	0.16 ± 0.02	0.24 ± 0.04	0.26 ± 0.03
	SMI	1.87 ± 0.09	1.99 ± 0.07	1.72 ± 0.05	1.74 ± 0.06
Diaphysis	Ct.V (mm^3)	2.35 ± 0.13	1.97 ± 0.10^{A}	2.58 ± 0.10	2.22 ± 0.12^{A}
	Ec.V (mm^3)	1.70 ± 0.09	1.76 ± 0.11	1.85 ± 0.15	1.89 ± 0.13
	Dp.V (mm^3)	4.05 ± 0.18	3.73 ± 0.19	4.41 ± 0.19	4.10 ± 0.19
	Ct.V/Dp.V (%)	58.5 ± 1.40	53.8 ± 0.99^{A}	60.0 ± 1.65	57.1 ± 3.22
	Ct.Th (μm)	275 ± 11.1	225 ± 5.6^{A}	266 ± 6.7	231 ± 12.7^{A}
	MOI (mm^4)	0.41 ± 0.09	0.34 ± 0.09^{A}	0.49 ± 0.10	0.42 ± 0.09^{A}
TRAP staining	N.Oc/BS (no./mm)	2.69 ± 0.21	4.37 ± 0.31^{A}	2.62 ± 0.05	3.55 ± 0.49
	Oc.S/BS (%)	11.0 ± 1.03	15.6 ± 0.81^{A}	10.5 ± 1.37	12.3 ± 1.19
Serum values	OC (ng/ml)	126 ± 12	155 ± 10^{A}	100 ± 9	131 ± 11^{A}
	ALP (nmol/min/ml)	225 ± 20	227 ± 14	205 ± 15	248 ± 23

Microcomputed tomography measurements in the femoral head (trabecular bone) and the diaphysis (cortical bone) of *TRPV5*$^{+/+}$ and *TRPV5*$^{-/-}$ mice as well as measurements deduced from TRAP staining of bone sections and serum values of osteocalcin (OC) and alkaline phosphatase (ALP). Values are expressed as means ± SEM. $^{A}P < 0.05$, significant difference between *TRPV5*$^{+/+}$ and *TRPV5*$^{-/-}$ mice, irrespective of sex (general linear regression model) (SPSS 10.0; SPSS Inc., Chicago, Illinois, USA).

pump extrude Ca^{2+} to the blood compartment, completing the process of transcellular Ca^{2+} transport (4). The expression of the Ca^{2+} transport proteins in the kidney was investigated by quantitative real-time PCR as described previously (13). Inactivation of the *TRPV5* gene was accompanied by a decrease in calbindin-D_{28K} and NCX1 mRNA levels (Figure 3d). As transcellular Ca^{2+} reabsorption in the distal convolution was abolished in *TRPV5*$^{-/-}$ mice, the concomitant decrease in calbindin-D_{28K} and NCX1 mRNA levels in the presence of elevated 1,25-$(OH)_2D_3$ levels suggests a regulatory mechanism controlled primarily by TRPV5. Thus, TRPV5 or the Ca^{2+} influx through TRPV5 possibly controls the transcription of the other Ca^{2+} transport genes, including calbindin-D_{28K} and NCX1. These findings emphasize the gatekeeper function of TRPV5. Although downregulation of renal calbindin-D_{28K} is secondary to TRPV5 ablation in the *TRPV5*$^{-/-}$ mice, the reduced calbindin-D_{28K} level may further augment the severity of the hypercalciuria. Interestingly, calbindin-D_{28K} knockout mice fed a Ca^{2+} diet (1% weight/volume) displayed an approximately twofold increase in urinary Ca^{2+} excretion compared with that of their wild-type littermates (26), whereas *TRPV5*$^{-/-}$ mice fed the same Ca^{2+} diet excreted about six times more Ca^{2+} in their urine than did their littermates.

In contrast to the excessive renal Ca^{2+} wasting noted, natriuresis and kaliuresis were not observed in the knockout mice, demonstrating the specific effect of TRPV5 inactivation on Ca^{2+} reabsorption (Figure 2d). Importantly, despite renal Ca^{2+} wasting, the serum Ca^{2+} concentration remained normal, suggesting successful compensatory mechanisms (Figure 4d). We investigated whether the impairment of transcellular Ca^{2+} reabsorption indirectly affected intestinal Ca^{2+} absorption. Active Ca^{2+} uptake by the small intestine is favored as compensation for renal Ca^{2+} wasting. To provide functional evidence for intestinal hyperabsorption in *TRPV5*$^{-/-}$ mice, we assessed Ca^{2+} absorption by measuring serum $^{45}Ca^{2+}$ at early time points after oral gavage, as described (14). A significant increase in the rate $^{45}Ca^{2+}$ absorption was observed in *TRPV5*$^{-/-}$ mice compared with their wild-type littermates, indicating a compensatory role for the small intestine (Figure 3c). Of note, this may actually represent an underestimation due to the applied single-$^{45}Ca^{2+}$-isotope technique used instead of a dual-isotope technique (27). Whereas TRPV5 is expressed predominantly in the kidney, TRPV6 is highly expressed in small intestine and has been implicated as the Ca^{2+} influx mechanism in enterocytes (1, 2). To test this hypothesis, duodenal RNA was extracted from knockout and wild-type littermates and analyzed for expression of TRPV6 and calbindin-D_{9K} by quantitative real-time PCR analysis. TRPV6 and calbindin-D_{9K} expression levels were significantly upregulated in *TRPV5*$^{-/-}$ mice, consistent with an increased Ca^{2+} absorption (Figure 3, c and e).

Serum 1,25-$(OH)_2D_3$ levels were significantly elevated in *TRPV5*$^{-/-}$ mice (Figure 4d), which explains the compensatory increased intestinal TRPV6 and calbindin-D_{9K} mRNA expression and Ca^{2+} absorption. The *TRPV5*$^{-/-}$ mouse is the first model to our knowledge to have sustained highly elevated 1,25-$(OH)_2D_3$ levels while remaining normocalcemic (Figure 4d) and normophosphatemic, as serum phosphate was not different between the *TRPV5*$^{+/+}$ and *TRPV5*$^{-/-}$ mice (2.68 ± 0.29 and 3.04 ± 0.18 mM, respectively, $n = 6$, $P > 0.2$). The elevated 1,25-$(OH)_2D_3$

levels observed in vitamin D receptor (VDR)-null mice (14) and in rickets type II are normally accompanied by hypocalcemia and increased serum PTH levels. In contrast, in *TRPV5*$^{-/-}$ mice with normal functioning VDRs, PTH was not significantly changed (Figure 4d). The elevated 1,25-$(OH)_2D_3$ levels in *TRPV5*$^{-/-}$ mice were not due to increased expression of renal 25-hydroxyvitamin D_3-1α-hydroxylase mRNA, since no differences were measured in the expression of this enzyme between *TRPV5*$^{+/+}$ and *TRPV5*$^{-/-}$ mice (100 ± 13% and 139 ± 29%, respectively; $n = 4$, $P > 0.2$). Studies to clarify the role of 1,25-$(OH)_2D_3$ in bone have been hampered by the complexity of distinguishing between disturbances in Ca^{2+} homeostasis and changes in serum 1,25-$(OH)_2D_3$ levels. Normal PTH plus normocalcemia make the *TRPV5*$^{-/-}$ mouse a unique model to study the effect of 1,25-$(OH)_2D_3$ on bone.

The homeostasis of bone tissue is maintained by the balanced processes of bone resorption and formation. The bone formation marker alkaline phosphatase was not different between the groups (Table 1), while osteocalcin was slightly but significantly higher in sera of *TRPV5*$^{-/-}$ versus *TRPV5*$^{+/+}$ mice. Bone resorption was studied by TRAP staining of femoral bone sections, by measurement of osteoclast number and surface, and by measurement of urinary deoxypyridinoline. Both N.Oc/BS and Oc.S/BS were significantly increased in female *TRPV5*$^{-/-}$ mice, with males showing a similar trend (Table 1). Urinary deoxypyridinoline showed large variations and was not significantly different between *TRPV5*$^{-/-}$ and *TRPV5*$^{+/+}$ mice (66 ± 8 nmol/nmol creatinine and 92 ± 21 nmol/nmol creatinine, respectively; $n = 5$–9, $P > 0.2$).

Detailed microcomputed tomography analyses of the femur demonstrated that Tb.Th in the femoral head of *TRPV5*$^{-/-}$ mice was significantly reduced compared with that of *TRPV5*$^{+/+}$ mice (Table 1 and Figure 4, a and c). BV/TV was not different between the genotypes. This could not be explained by a difference in Tb.N (Table 1). Alternatively, it is possible that the trabeculae are longer, that is, they protrude further into the bone marrow cavity, and thereby compensate for reduced Tb.Th. CD and SMI were not altered in the femoral head, irrespective of phenotype and sex. Analyses of the diaphysis showed that Ct.V, Ct.V/Dp.V, and Ct.Th were significantly reduced in *TRPV5*$^{-/-}$ versus *TRPV5*$^{+/+}$ mice (Table 1 and Figure 4, a and c). Finally, the polar MOI was significantly reduced in *TRPV5*$^{-/-}$ mice, indicative of an altered geometrical distribution and reduced mechanical properties of the diaphyseal bone (Table 1 and Figure 4b). The observed changes in bone structure cannot be attributed to differences in body weight (Figure 2a). Also, the bone lengths of *TRPV5*$^{-/-}$ and *TRPV5*$^{+/+}$ mice were similar. In summary, the unchanged alkaline phosphatase together with the elevated N.Oc/BS and Oc.S/BS in the *TRPV5*$^{-/-}$ mice may explain the observed reduced trabecular and cortical thickness.

It is unclear whether the reduced Tb.Th and Ct.Th found in the *TRPV5*$^{-/-}$ mice is a direct effect of the genotype or results from prolonged elevated 1,25-$(OH)_2D_3$ levels. Interestingly, a recent study of long-term treatment of mice with 1,25-$(OH)_2D_3$ demonstrated a decrease in cortical thickness and cross-sectional area and a 50% reduction in stiffness (28), which is in line with the current observations. We hypothesize that the bone phenotype of the *TRPV5*$^{-/-}$ mice, due to prolonged elevated 1,25-$(OH)_2D_3$ levels, develops and progresses throughout life. However, at present it is premature to draw definitive conclusions about bone metabolism, and future experiments will certainly address this point in detail.

The epithelial Ca^{2+} channels TRPV5 and TRPV6 have been studied extensively in epithelial tissues controlling the Ca^{2+} homeostasis and exhibit a range of distinctive properties that distinguish them from other TRP channels (3, 4). TRP channels display an extraordinary assortment of selectivities and activation mechanisms, some of which represent previously unrecognized modes for regulating ion channels (3). Moreover, there is only limited information about the biological functions of TRP channels, which appear to be equally diverse and range from pain perception to male aggression. The present study demonstrated that the new TRP member TRPV5 is the gatekeeper in active Ca^{2+} reabsorption in the kidney. Ablation of the *TRPV5* gene seriously disturbs renal Ca^{2+} handling, resulting in compensatory intestinal hyperabsorption and bone abnormalities. These deficiencies in Ca^{2+} handling have been reported frequently in patients with idiopathic hypercalciuria, although the molecular basis for this disorder remains unknown. Dysfunction of TRPV5 may contribute to such disturbances of Ca^{2+} homeostasis, and the TRPV5 knockout mouse is, therefore, a powerful animal model for elucidating the molecular mechanism underlying idiopathic hypercalciuria. Finally, the increased 1,25-$(OH)_2D_3$ levels and effects on bone structure indicate that alterations in TRPV5 may have implications for age-related bone disorders, including osteoporosis.

Acknowledgments

This work was supported by the Dutch Organization for Scientific Research (Zon-Mw 016.006.001), an EMBO fellowship to J.G.J. Hoenderop, and National Science Foundation grants to E. Hummler and B.C. Rossier. The authors thank C.H. van Os, H.A.P. Pols, and P.M.T. Deen for stimulating discussions; K. Richter, D.Y. Huang, M. van Abel, and C.J. Buurman for technical assistance; R. Bouillon (Catholic University Leuven, Leuven, Belgium) for providing the osteocalcin antibody; and H. Westphal (National Institute of Child Health and Human Development, Bethesda, Maryland, USA) and J. van Es (Hubrecht Laboratory, Utrecht, The Netherlands) for providing the Ella-cre-deletor mice.

1. Hoenderop, J.G., et al. 1999. Molecular identification of the apical Ca^{2+} channel in 1, 25-dihydroxyvitamin D_3-responsive epithelia. *J. Biol. Chem.* **274**:8375–8378.
2. Peng, J.B., et al. 1999. Molecular cloning and characterization of a channel-like transporter mediating intestinal calcium absorption. *J. Biol. Chem.* **274**:22739–22746.
3. Montell, C., Birnbaumer, L., and Flockerzi, V. 2002. The TRP channels, a remarkably functional family. *Cell*. **108**:595–598.
4. Hoenderop, J.G., Nilius, B., and Bindels, R.J. 2002. Molecular mechanisms of active Ca^{2+} reabsorption in the distal nephron. *Ann. Rev. Physiol.* **64**:529–549.
5. Yue, L., Peng, J.B., Hediger, M.A., and Clapham, D.E. 2001. CaT1 manifests the pore properties of the calcium-release-activated calcium channel. *Nature*. **410**:705–709.
6. Radtke, F., et al. 1999. Deficient T cell fate specification in mice with an induced inactivation of Notch1. *Immunity*. **10**:547–558.
7. Hummler, E., et al. 1996. Early death due to defective neonatal lung liquid clearance in alpha-ENaC-deficient mice. *Nat. Genet.* **12**:325–328.
8. Lakso, M., et al. 1996. Efficient in vivo manipulation of mouse genomic sequences at the zygote stage. *Proc. Natl. Acad. Sci. U. S. A.* **93**:5860–5865.
9. Vallon, V. 2003. In vivo studies of the genetically modified mouse kidney. *Nephron. Physiol.* **94**:P1–P5.
10. Zhelyaskov, V.R., Liu, S., and Broderick, M.P. 2000. Analysis of nanoliter samples of electrolytes using a flow-through microfluorometer. *Kidney. Int.* **57**:1764–1769.
11. Muhlert, M., Julita, M., and Quamme, G. 1982. Disappearance of calcium and other electrolytes from microvolume samples. *Am. J. Physiol.* **242**:F202–F206.
12. Hoenderop, J.G., et al. 2003. Homo- and heterotetrameric architecture of the epithelial Ca^{2+} channels, TRPV5 and TRPV6. *EMBO J.* **22**:776–785.
13. Hoenderop, J.G., et al. 2002. Modulation of renal Ca^{2+} transport protein genes by dietary Ca^{2+} and 1,25-dihydroxyvitamin D_3 in 25-hydroxyvitamin D_3-1alpha-hydroxylase knockout mice. *FASEB J.* **16**:1398–1406.
14. van Cromphaut, S., et al. 2001. Active duodenal calcium absorption in vitamin D receptor-knock out mice: functional and molecular aspects. *Proc. Natl. Acad. Sci. U. S. A.* **98**:13324–13329.
15. Parfitt, A.M., et al. 1987. Bone histomorphometry: standardization of nomenclature, symbols, and units. Report of the ASBMR Histomorphometry Nomenclature Committee. *J. Bone Miner. Res.* **2**:595–610.
16. Hildebrand, T., and Ruegsegger, P. 1997. A new method for the model-independent assessment of thickness in three-dimensional images. *J. Microscopy*. **185**:67–75.
17. Odgaard, A., and Gundersen, H.J. 1993. Quantification of connectivity in cancellous bone, with special emphasis on 3-D reconstructions. *Bone*. **14**:173–182.
18. Hildebrand, T., and Ruegsegger, P. 1997. Quantification of bone microarchitecture with the structure model index. *Comput. Methods. Biomech. Biomed. Engin*. **1**:15–23.
19. Cole, A.A., and Walters, L.M. 1987. Tartrate-resistant acid phosphatase in bone and cartilage following decalcification and cold-embedding in plastic. *J. Histochem. Cytochem*. **35**:203–206.
20. Zolotnitskaya, A., and Satlin, L.M. 1999. Developmental expression of ROMK in rat kidney. *Am. J. Physiol*. **276**:F825–F836.
21. Sands, J.M., et al. 1997. Apical extracellular calcium/polyvalent cation-sensing receptor regulates vasopressin-elicited water permeability in rat kidney inner medullary collecting duct. *J. Clin. Invest*. **99**:1399–1405.
22. Frick, K.K., and Bushinsky, D.A. 2003. Molecular mechanisms of primary hypercalciuria. *J. Am. Soc. Nephrol*. **14**:1082–1095.
23. Puliyanda, D.P., Ward, D.T., Baum, M.A., Hammond, T.G., and Harris, H.W., Jr. 2003. Calpain-mediated AQP2 proteolysis in inner medullary collecting duct. *Biochem. Biophys. Res. Commun*. **303**:52–58.
24. Miller, L.A., and Stapleton, F.B. 1989. Urinary volume in children with urolithiasis. *J. Urol*. **141**:918–920.
25. Baumann, J.M. 1998. Stone prevention: why so little progress? *Urol. Res*. **26**:77–81.
26. Sooy, K., Kohut, J., and Christakos, S. 2000. The role of calbindin and 1,25dihydroxyvitamin D_3 in the kidney. *Curr. Opin. Nephrol. Hypertens*. **9**:341–347.
27. Hillman, L.S., Tack, E., Covell, D.G., Vieira, N.E., and Yergey, A.L. 1988. Measurement of true calcium absorption in premature infants using intravenous ^{46}Ca and oral ^{44}Ca. *Pediatr. Res*. **23**:589–594.
28. Smith, E.A., et al. 2000. Effects of long-term administration of vitamin D_3 analogs to mice. *J. Endocrinol*. **165**:163–172.